PERGAMON

International Journal of Heat and Mass Transfer 44 (2001) 2903–2916

International Journal of HEAT and MASS TRANSFER

www.elsevier.com/locate/ijhmt

Establishing heat–entropy analogies for interface tracking in phase change heat transfer with fluid flow

G.F. Naterer *

Department of Mechanical and Industrial Engineering, University of Manitoba, 15 Gillson Street, Winnipeg, Man., Canada R3T 2N2

Received 27 March 2000; received in revised form 9 October 2000

Abstract

In this paper, entropy is presented as an important variable in effectively describing and predicting various phase change processes. An interfacial entropy constraint, downward concavity condition and Second Law formulation are obtained. Modelling of interfacial momentum interactions and thermal recalescence are based on heat–entropy analogies. It is shown that deeper insight into phase change processes with fluid flow can be realized through consideration of the analogy variable (entropy). Also, an entropy-based approach provides effective guidelines for interface tracking and numerical stability in phase change computations involving a control volume-based finite element method (CVFEM) formulation.

1. Introduction

Solidification and melting arises in many important applications, including materials processing, ice accretion on structures and thermal energy storage in electronic assemblies. The design and prediction of these phase change processes typically involves solutions of the conservation equations (i.e. mass, momentum, energy, species concentration equations). A variety of numerical procedures, such as finite differences [1], finite elements [2], finite volumes [3] and combined finite volume–element methods [4,5], has been developed for these problems. These numerical models provide effective tools for further understanding of complicated transport processes during solidification and melting.

Additional recent studies have examined specific transport processes during solid–liquid phase change, such as solute segregation, thermosolutal convection and interdendritic and shrinkage flows. For example, Flood and Davidson [6] observed the formation of centerline macrosegregation in aluminum cast ingots including the sensitivity to ingot thickness and casting speed. Rady and co-workers [7] used a finite volume method to predict thermal and solutal buoyancy during solidification of hypereutectic and hypoeutectic binary alloys. Additional phenomena involving interdendritic flows, particularly solute redistribution in the mushy zone, were examined by Maples and Poirier [8]. Solidification shrinkage flows were examined by Naterer [9] through a simultaneous pressure–velocity coupling in the two-phase zone. Many diverse aspects of modelling developments in these phase change problems are summarized and discussed in a comprehensive review by Salcudean and Abdullah [10].

Although significant advances have been achieved in the analysis of the conservation equations, the corresponding consideration of entropy (both physical and computational) in solidification and melting problems has been sparse. Computational entropy refers to the discretized approximation of entropy as a state variable, while physical entropy represents the actual thermodynamic entropy, or entropy production, arising from a physical process such as heat transfer or viscous mixing. Bejan [11] examines minimization of entropy generation in applications such as refrigeration, energy storage systems and power generation. Charach and Rubinstein [12] investigate entropy generation during phase change heat conduction.

In solid–liquid phase change problems, entropy can serve as an effective parameter for understanding and

* Tel.: +1-204-474-9804; fax: +1-204-275-7507.
E-mail address: natererg@cc.umanitoba.ca (G.F. Naterer).

0017-9310/01/$ - see front matter
PII: S0017-9310(00)00334-3

Nomenclature

C	solute concentration (pct. weight)
D	mass diffusivity (m^2/s)
e	internal energy (J/kg)
f	mass fraction
$\mathbf{F}_b$	body force (N)
g	gravitational acceleration (m/s^2)
k	thermal conductivity (W/m K)
n	normal to interface
$\dot{P}$	production rate
S	entropy or source term
t	time (s)
T	temperature (K)
$\mathbf{v}$	velocity (m/s)

Greek symbols

β	expansion coefficient
μ	viscosity (kg/ms)
ρ	density (kg/m^3)

Subscripts

e	eutectic
ip	integration point
k	phase k
l	liquid
s	solid or entropy

Superscripts

n	previous time level
$n+1$	current time level

describing various physical processes. For example, interface properties, such as interface "roughness", are determined from the entropy change during phase transition. At microscopic scales, a rough or "non-faceted" surface exhibits a low entropy of fusion. During solidification, dendritic arms often grow in a direction corresponding to the maximum thermal irreversibility since it is aligned with the heat flow direction (i.e. direction of local temperature gradient). As a result, entropy is an important characteristic of the two-phase permeability in describing how pockets or channels of liquid are formed within the solid matrix. In addition, thermal recalescence involves a transient temperature rise during cooling of a freezing crystal that occurs due to a latent heat release which exceeds the other modes of cooling. In this case, a positive rate of entropy change can indicate the duration and magnitude of the local reheating. Although these processes have been observed by many researchers, less attention has been given to the role of entropy. It is anticipated that entropy can serve as an effective variable in describing these physical processes.

Also, previous studies of computational fluid dynamics have shown that the Second Law of Thermodynamics can identify proper solution trends (i.e. [13]) and upwinding accuracy (i.e. [14]). In the context of phase change heat transfer, these results may establish the uniqueness of interface resolution subject to different convergence tolerances imposed on a numerical model. Entropy production can also determine an optimal and convergent phase distribution during numerical iterations without randomly cycling through phases because only entropy-producing solutions are physically possible. The use of arbitrary convergence tolerances can be reduced or eliminated with the Second Law. Based on previous entropy studies by Naterer and Schneider [15], it may be feasible to develop a quantitative approach to numerical stability and error analysis through the Second Law. In this paper, we will consider the modelling of entropy transport for anticipated benefits in the computational analysis of solidification and melting with natural convection.

In fixed grid methods for phase change problems, the location of the solid–liquid interface is determined by an application of appropriate conservation principles and the latent heat of phase change is apportioned between the nearest nodal points in the model. In this approach, the location of the phase interface can only be resolved with confidence to within one mesh spacing. An iterative procedure is required as a result of non-linearities in the interfacial constraints (i.e. energy balance across phase interface), as well as convection terms in the momentum equations. These iterations are typically performed until changes in the solution between successive iterations decline below a specified (often arbitrary) tolerance level (i.e. Picard iteration). Numerous techniques have been developed for convergence acceleration in non-linear problems, including relaxation factors and multigrid methods [16]. Interface tracking by sequential steps was proposed by Schneider and Raw [17] whereby two phase rules are used to coordinate the orderly progression of phase transition between adjacent control volumes. The approach was later extended to binary constituent problems and validated through experimentation by Naterer and Schneider [4,5,18]. It will be shown that these iterative procedures are closely related to the Second Law. In establishing this relationship, further improvements in computational performance, such as convergence acceleration during interface tracking, may be realized.

The main objective of this paper is to attempt to derive an alternative entropy-based framework (so-called "heat–entropy analogies") for various transport

processes during phase change. These transport processes include inter-phase momentum and recalescence phenomena. The intrinsic generality of entropy as an abstract concept (i.e. applications ranging from physical systems to information and signal theories) provides opportunities for deeper insight into complicated phenomena. Previous analogies have established connections between heat transfer and friction coefficients (i.e. Reynolds analogy between heat and momentum) and similar opportunities may be established with entropy. It will be shown that transport phenomena involving one variable (temperature) may be inferred through consideration of the other analogy variable (entropy). This type of similarity can be useful if predicting a particular variable is difficult or time-consuming, whereas analysis involving the other analogy variable may be more readily implemented. Furthermore, benefits arising from the Second Law in computational models, such as numerical stability, may be realized. In summary, it is anticipated that the pursuit of heat–entropy analogies is a worthwhile endeavour.

2. Formulation

The formulation of solid–liquid phase change, including the governing equations, interfacial constraints and numerical model, will be discussed in this section.

2.1. Governing equations

The governing equations for solid–liquid phase transition are the conservation equations (i.e. mass, momentum, energy), in conjunction with the binary alloy phase diagram, equation(s) of state and appropriate supplementary equations relating microscopic and macroscopic quantities. Continuum equations can be written for the conserved quantities, ξ_k, where ξ_k refers to a vector of conserved quantities, including mass and energy, and the subscript k refers to phase k, i.e. $k = 1$ (solid) and $k = 2$ (liquid). Then, the mixture equations are obtained by summing the individual continuum equations over both phases within a control volume, including solid and liquid phases, and rewriting the variables in terms of mixture variables. A mixture quantity is defined as the mass fraction-weighted sum of individual phase components. For example,

$$\mathbf{v} = f_l \mathbf{v}_l + f_s \mathbf{v}_s, \tag{1}$$

$$k = f_l k_l + f_s k_s \tag{2}$$

refer to the mixture velocity and thermal conductivity, respectively. If a conserved quantity is written without a subscript involving phase, then it refers to a mixture quantity.

After performing the summation of conservation equations over both phases, the mixture equations for mass and momentum, respectively, can be expressed in the following manner:

$$\frac{\partial \rho}{\partial t} + \nabla \cdot (\rho \mathbf{v}) = 0, \tag{3}$$

$$\frac{\partial (\rho \mathbf{v})}{\partial t} + \nabla \cdot (\rho \mathbf{v}\mathbf{v}) = -\nabla p + \nabla \cdot \left(\frac{\rho_l}{\rho} \mu_l \nabla \mathbf{v} \right) + \mathbf{F}_b + \mathbf{F}_p, \tag{4}$$

where $\mathbf{F}_b$ and $\mathbf{F}_p$ refer to body forces and phase interaction forces, respectively. In the present analysis, the body forces, $\mathbf{F}_b$, are given by

$$\mathbf{F}_b = \rho \mathbf{g} \beta_T (T - T_0) + \rho \mathbf{g} \beta_C (C - C_0), \tag{5}$$

where $\mathbf{g}$, β_T and β_C represent the gravity vector and thermal and solutal expansion coefficients, respectively. The phase interaction forces, $\mathbf{F}_p$ will be determined from appropriate supplementary relations (described in subsequent section).

The remaining conservation equations for species and energy, respectively, are given by

$$\frac{\partial (\rho C)}{\partial t} + \nabla \cdot (\rho \mathbf{v} C) = \nabla \cdot (\rho_l f_l D_l C_l + \rho_s f_s D_s C_s) + \nabla \cdot (\rho C - \rho C_l)\mathbf{v}, \tag{6}$$

$$\frac{\partial (\rho h)}{\partial t} + \nabla \cdot (\rho \mathbf{v} h) = \nabla \cdot (k \nabla T) + \nabla \cdot (\rho h - \rho h_l)\mathbf{v}, \tag{7}$$

where h refers to enthalpy. In phase k, this enthalpy is written as

$$h_k(C, T) = \int_{T_0}^{T} c_{r,k}(\zeta)\, d\zeta + h_{r,k}(C, T). \tag{8}$$

In Eq. (8), $c_{r,k}(T)$ refers to the reference specific heat of phase k. The final terms in Eqs. (6) and (7) are included in that fashion to indicate their evaluation as source terms, S_c and S_e, respectively, in a conventional numerical formulation. The above governing equations will be solved in conjunction with the phase equilibrium diagram (see Fig. 1).

In addition, the following assumptions will be adopted for closure of the overall model:

- a continuous liquid–solid mixture exists without internal gas voids;
- two-dimensional, incompressible, laminar, Newtonian flow;
- stationary solid phase during phase transition;
- binary constituent phase transition above the eutectic temperature (see Fig. 1);
- variations of thermophysical properties, such as thermal conductivity, in terms of concentration or temperature will be neglected;

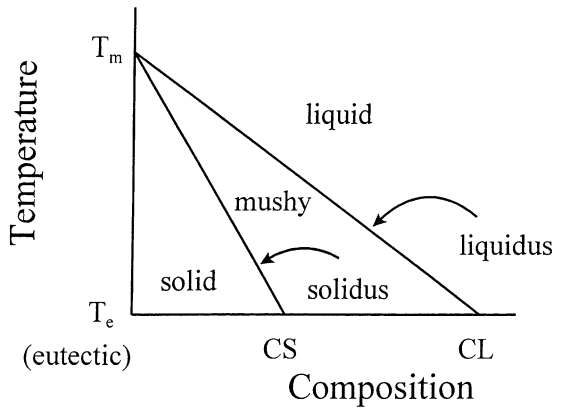

Fig. 1. Binary alloy phase diagram.

- diffusion-based relationship relating liquid fraction, temperature and solute concentration in the two-phase zone [4].

In addition to the conservation equations, interfacial constraints will be required for balances of conserved quantities and entropy across the moving phase interface.

2.2. Interfacial constraints

Interface tracking typically requires iterative solutions because the interface position is often unknown and its motion exhibits a strongly non-linear character. The interfacial constraints will be utilized in conjunction with entropy as a basis for effective interface tracking. The binary phase diagram will be used to determine the equilibrium temperature and concentration at the solid–liquid interface. In Fig. 2, a typical schematic of the solid–liquid interface is illustrated (note: n, V_i, $\mathrm{d}A$ and $\mathrm{d}f_s\mathrm{d}V$ refer to normal direction, interface velocity, area and solid fraction increment multiplied by change in volume).

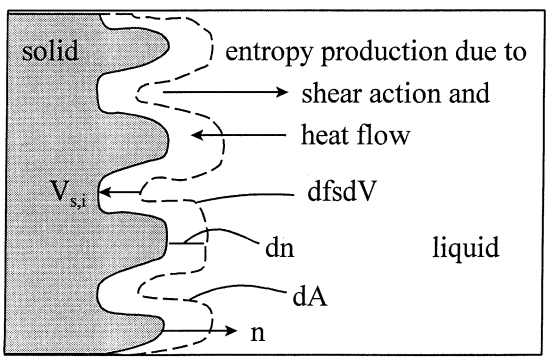

Fig. 2. Schematic of phase interface.

2.2.1. Energy

The heat transfer from the liquid phase into the phase interface, $\mathrm{HT_l}$, consists of conduction (Fourier's law) and advection components,

$$\mathrm{HT_l} = -k_\mathrm{l}\,\mathrm{d}A\left.\frac{\mathrm{d}T}{\mathrm{d}n}\right|_\mathrm{l}\mathrm{d}t + \rho_\mathrm{l}V_\mathrm{l}e_\mathrm{l}\,\mathrm{d}A\,\mathrm{d}t. \tag{9}$$

A similar heat transfer expression can be written in the solid phase. Also, considering a control volume at the phase interface with a thickness $\mathrm{d}n$, then the change of energy that accompanies the advance of the interface arises from the energy difference of an entirely liquid volume, $\mathrm{d}A\,\mathrm{d}n$, and a final solid volume, i.e.

$$\mathrm{d}E \equiv \mathrm{HT_l} - \mathrm{HT_s} = \rho_\mathrm{l}e_\mathrm{l}\,\mathrm{d}A\,\mathrm{d}n - \rho_\mathrm{s}e_\mathrm{s}\,\mathrm{d}A\,\mathrm{d}n. \tag{10}$$

Based on these results in Eqs. (9) and (10), it can be shown that the interfacial energy constraint is obtained as

$$-k_\mathrm{l}\left.\frac{\mathrm{d}T}{\mathrm{d}n}\right|_\mathrm{l} + k_\mathrm{s}\left.\frac{\mathrm{d}T}{\mathrm{d}n}\right|_\mathrm{s} = -V_\mathrm{s}\rho_\mathrm{s}\Delta e_\mathrm{f} + \rho_\mathrm{s}\Delta e_\mathrm{f}V_\mathrm{i}, \tag{11}$$

where $\Delta e_\mathrm{f} = e_\mathrm{l} - e_\mathrm{s}$ is the latent heat of fusion and V_i refers to the interface velocity. The lower case symbol for internal energy, e, refers to intensive (specific) variable, whereas the upper case notation denotes extensive variables. In the present studies, the solid phase will be assumed stationary such that the first term on the right-hand side of Eq. (11) is neglected.

2.2.2. Other conserved variables

In a similar manner as the above interfacial equation for energy, the interfacial constraints for the other conserved variables, such as mass, solute concentration and momentum, can be obtained by appropriate balances across the phase interface. For example, in a similar way as the energy equation, the interfacial relation for the concentration of component c in a multi-component mixture, C_c, is obtained as follows:

$$-\rho_\mathrm{l}D_\mathrm{l}\left.\frac{\mathrm{d}C_\mathrm{c}}{\mathrm{d}n}\right|_\mathrm{l} + \rho_\mathrm{s}D_\mathrm{s}\left.\frac{\mathrm{d}C_\mathrm{c}}{\mathrm{d}n}\right|_\mathrm{s} = -V_\mathrm{s}\rho_\mathrm{s}C_\mathrm{c,ls} + \rho_\mathrm{s}C_\mathrm{c,ls}V_\mathrm{i}, \tag{12}$$

where the difference between phase concentrations, $C_\mathrm{c,ls} = C_\mathrm{c,l} - C_\mathrm{c,s}$, is obtained from the binary phase equilibrium diagram (see Fig. 1).

The previous interfacial results were obtained for conserved quantities, such as energy. However, entropy is not a conserved quantity since it can be produced (but never destroyed in an isolated system). The following development of the entropy interfacial constraint will account for entropy production during irreversible processes with solid–liquid phase change.

2.2.3. Entropy

In the case of entropy transport, we have the following transport equation in phase k:

$$\frac{D(f_k\rho_k s_k)}{Dt} = \nabla\cdot\left(\frac{f_k k_k \nabla T}{T}\right) + \nabla\cdot\left(\sum_{c=1}^{N}\frac{f_k\zeta_{c,k}\mathbf{j}_{c,k}}{T}\right) + \dot{P}_{s,k}, \tag{13}$$

where $\dot{P}_{s,k}$ refers to the entropy production rate and $\zeta_{c,k} = \partial e_k/\partial C_{c,k}$ is the chemical potential of constituent c in phase k. It can be interpreted as an additional increase of work potential in the fluid if $dC_{c,k}$ of constituent c is added to the mixture. On the right-hand side of Eq. (13), the terms represent the entropy flow with heat flux and species (mass) flux, $\mathbf{j}_{c,k}$, and the entropy production rate, respectively.

Since entropy is not measured directly, we need an additional relationship involving entropy and the conserved quantities, such as energy (or temperature), solute concentration, etc. In particular, we have the following Gibbs equation for a multicomponent mixture in terms of phase k:

$$ds_k = \frac{de_k}{T} + \frac{p\,dv_k'''}{T} - \sum_{c=1}^{N}\frac{\zeta_{c,k}\,dC_{c,k}}{T}, \tag{14}$$

where v''' represents specific volume. A latent heat term is not included in Eq. (14) because the equation is written within the single phase k.

Assuming an incompressible substance in each phase, rewriting Eq. (14) in terms of a substantial derivative and rearranging terms,

$$T\frac{D(f_k\rho_k s_k)}{Dt} = \frac{D(f_k\rho_k e_k)}{Dt} - \sum_{c=1}^{N} g_{c,k}\frac{D(f_k\rho_k C_{c,k})}{Dt}. \tag{15}$$

Substituting appropriate terms from Eqs. (6) and (7) into the above equation, we have

$$\frac{D(f_k\rho_k s_k)}{Dt} = \frac{1}{T}\left\{k_k\nabla^2 T + \tau\cdot\nabla\mathbf{v}_k + \dot{P}_{e,k}\right\} - \frac{1}{T}\sum_{c=1}^{N}\zeta_{c,k}\left\{-\nabla\cdot\mathbf{j}_{c,k} + \dot{P}_{c,k}\right\}. \tag{16}$$

Expanding the divergence terms in this equation using the product rule and comparing the resulting equation to Eq. (13), we obtain the following result for the entropy production in phase k:

$$\dot{P}_{s,k} = \frac{f_k k_k(\nabla T)^2}{T^2} + \frac{\mu\Phi}{T} + \frac{\dot{P}_{e,k}}{T} - \frac{1}{T}\sum_{c=1}^{N}\mathbf{j}_{c,k}\cdot\nabla\zeta_{c,k} + \frac{1}{T^2}\sum_{c=1}^{N}\zeta_{c,k}\mathbf{j}_{c,k}\cdot\nabla T - \sum_{c=1}^{N}\frac{\zeta_{c,k}\dot{P}_{c,k}}{T}. \tag{17}$$

The production terms on the right-hand side of Eq. (17) vanish after summation over the phases because production/destruction of energy or species in one phase is accompanied by destruction/production in the other phase. However, the same explanation does not apply to entropy because processes such as heat transfer, viscous dissipation and fluid mixing are irreversible and thus produce entropy within an individual phase.

The entropy interfacial constraint can also be written in terms of the local entropy production rate at the phase interface. The entropy transfer from the liquid phase into the interface, ET_l, may be written as

$$ET_l = -k_l\frac{dA}{T}\frac{dT}{dn}\,dt + \rho_l V_l s_l\,dA\,dt, \tag{18}$$

which consists of entropy flow arising from heat conduction as well as advection, since liquid flow carries entropy into the interface. A similar expression, ET_s, can be obtained for the solid phase. Also, in an analogous manner as the energy analysis, the entropy difference between a liquid volume, $dA\,dn$, at the interface, and a subsequent solidified volume, can be written as

$$\begin{aligned} dS &= \rho_l s_l\,dA\,dn - \rho_s s_s\,dA\,dn \\ &= ET_l - ET_s + \rho_l P_{s,i}\,dA\,dn, \end{aligned} \tag{19}$$

where the interfacial entropy production, $P_{s,i}$, accounts for the entropy produced per unit mass due to heat transfer and shear action along the dendrite arms as the dendrite moves a distance dn during the time interval dt.

Combining the above equations and rearranging terms,

$$(\rho_l s_l - \rho_s s_s)\frac{dn}{dt} = -\frac{k_s}{T_l}\frac{dT}{dn}\bigg|_l + \frac{k_s}{T_s}\frac{dT}{dn}\bigg|_s + \rho_l V_l s_l - \rho_s V_s s_s + \rho_l P_{s,i}\frac{dn}{dt}. \tag{20}$$

Combining this equation with continuity, we obtain the following result for the entropy production at the phase interface (i.e. interfacial entropy constraint),

$$P_{s,i} = \frac{\rho_s}{\rho_l}\left(\Delta s_f - \frac{\Delta e_f}{T}\right) + \frac{k_l}{\rho_l V_i}\frac{dT}{dn}\bigg|_l\left(\frac{1}{T_l} - \frac{1}{T_s}\right), \tag{21}$$

where $\Delta s_f = s_l - s_s$ refers to the entropy of fusion. Experiments have shown that the entropy of fusion is approximately constant for most metals and alloys, $\Delta s_f \approx 8.4$ J/mol K. The lower case symbol for entropy, s, refers to intensive (specific) variable, whereas the upper case notation will refer to the extensive variable. Richard's Rule states that the entropy of fusion is also approximately equal to the heat of fusion divided by the phase change temperature.

In addition, entropy as a function of the conserved variables, ξ, is bounded from above. Entropy is produced during irreversible processes, and the entropy function, $S(\xi)$, reaches a maximum value at an equilibrium state. As a result, $S(\xi)$ is a downward concave function, i.e.

$$S''(\xi) < 0, \tag{22}$$

where the prime notation refers to differentiation. In other words, $S''(\xi)$ must be a negative definite matrix because irreversible processes produce entropy.

2.3. Numerical procedure

Analysis of the entropy equations, heat–entropy analogies (following sections) and the Second Law of Thermodynamics will be performed in the present paper. In the numerical formulation, the problem domain is subdivided into finite elements and control volumes. A control volume is defined by all sub-elements (or sub-control volumes, SCVs) surrounding a particular node and an integration point (ip) is located at the midpoint of each sub-surface (SS). Local coordinates (s, t) are defined within each element. Isoparametric, linear shape functions are used within each element to represent the variation of the dependent scalar variables in terms of nodal variables.

Then, a control volume-based finite element method (CVFEM), based on the PHASES algorithm [4,5], is adopted for the solution of the phase change conservation equations and extended here to the present entropy formulation. For details about the CVFEM and PHASES, as well as computational accuracy tests, see [4,5].

3. The Second Law and heat–entropy analogies

At this stage, the use of entropy as a "variable", "parameter" and/or "property" should be elucidated. From a physical perspective, entropy is a thermodynamic property that describes the degree of randomization in a gas, liquid or solid at the microscopic scale. In this definition, entropy can be produced, but never destroyed in an isolated system. Unlike physical processes, computational procedures may artificially produce or destroy entropy due to discretization errors or other factors. In the latter case, the meaning of entropy as a property is questioned since violations of the Second Law are not observed. Despite these violations, previous research has shown that the computational entropy can still provide a useful parameter in achieving numerical stability and improved computational accuracy. We will refer to the entropy "variable" as a combined physical "property" and computational "parameter".

It is anticipated that the main contribution of the present work is to establish an entropy-based framework (so-called "heat–entropy analogies"), involving both computational and physical aspects of transport processes during phase change. In a similar way to benefits realized by previous analogies, such as the Reynolds analogy between heat and momentum, the present research explores the opportunities of introducing entropy in phase change problems. The theory involves the governing equations, i.e. Eqs. (3), (4), (6), (7), and (13), subject to suitable boundary conditions. These boundary conditions are identified through specific cases in application problems.

In this section, entropy will be considered as an important variable in the following parts of the phase change analysis:

1. numerical discretization;
2. supplementary relations;
3. local reheating;
4. numerical iterations;
5. non-linear stability.

It is anticipated that entropy can serve as an effective variable in providing further insight into difficulties often encountered with the analysis of phase change problems.

3.1. Numerical discretization

Entropy and entropy production will be obtained from the following formulation of the Second Law of Thermodynamics. In phase k, the Second Law may be written as

$$\dot{P}_s \equiv \frac{\partial S_k}{\partial t} + \nabla \mathbf{G}_k \geqslant 0, \tag{23}$$

where $S(\xi_k)$ and $\mathbf{G}(\xi_k)$ represent the entropy and entropy flux in phase k, respectively. In Eq. (23), the extensive variable, S_k, may be replaced by density multiplied by specific entropy, ρs_k (i.e. introduces intensive variable). The intensive variable, s_k, also appears in the entropy flux; for example, $\rho_k \mathbf{v} s_k$ gives the advective component of the entropy flux in Eq. (23).

After the solution of the conservation equations is obtained, an additional step is required to estimate the entire spatial distribution of the conserved variables, $\xi(\mathbf{x}, t)$, based on nodal and integration point values, so that $S(\xi_k)$ and $\mathbf{G}(\xi_k)$ can be properly evaluated in Eq. (23). Since the choice of a uniform entropy suggests a type of quasi-equilibrium condition, then we will assume that $\xi = \xi_i$ within a finite volume, where the subscript i refers to node i, in order to ensure the Second Law is not violated during the reconstruction step. In addition to assuming that ξ is piecewise constant within a control volume, it is assumed as piecewise constant, at its integration point value, along each control surface. These conserved variables can then be used in the evaluation of entropy.

In the finite element-volume framework, the discretized form of the Second Law in Eq. (23) is obtained by a backward difference in time for the transient derivative and integration point approximations for the surface flux terms [19]. The computation of the transient term requires an entropy equation of state. An integrated and discretized form of the Gibbs equation is used to obtain a piecewise logarithmic equation of state. In this model,

entropy varies with temperature and concentration and an entropy of fusion is released or absorbed during phase change. This procedure completes the closure of the equation of state. In addition, supplementary relations, including two-phase momentum interactions, $\mathbf{F}_p$, in Eq. (4), are required for closure of the overall formulation.

3.2. Supplementary relations

In the modelling of the two-phase momentum equations, a supplementary relation for the momentum phase interactions, $\mathbf{F}_p$, is required for closure of the governing equations. For fluid flow through a porous medium, Darcy's law [20], $\mathbf{F}_p K = v f_l(\mathbf{v}_l - \mathbf{v}_s)$, may be employed for the phase interaction force dependence on porous medium permeability, K, and liquid fraction, f_l. In the application of Darcy's law, a fixed dendritic section (porous medium) is required, i.e. not freely moving or settling crystals. The assumption of stationary solid material (i.e. $\mathbf{v}_s = 0$) in the governing equations remains consistent with Darcy's law.

Previous models of solid–liquid phase change have often used the Blake–Kozeny equation [20] for the solid permeability [3],

$$K = K_0 \left[\frac{f_l^3}{(1-f_l)^2} \right], \tag{24}$$

where K_0 is an empirical coefficient. This model was developed through a physical analogy between interdendritic flow and Hagen–Poiseuille viscous flow [20] through a non-circular tube with an equivalent hydraulic radius based on the local liquid fraction (see Fig. 3(a)).

However, at high values of f_l (i.e. $f_l > 0.5$ [3]), a cross-flow perpendicular to dendrite arms may produce a higher pressure difference than the Blake–Kozeny prediction because of wake interactions and interdendritic viscous effects. As a result, an alternative model was developed to account for these cross-flow effects [4], i.e.

$$K = K_0 \left(\frac{f_l}{\sqrt{1-f_l}} \right). \tag{25}$$

It can be readily shown that both Eqs. (24) and (25), as well as the resulting Eq. (4), approach the proper limits as $f_l \to 0$ (solid) and $f_l \to 1$ (liquid).

In previous studies [4], a flow alignment factor, χ, was adopted to represent a weighting factor between the axial relation, Eq. (24), and the cross-flow relation, Eq. (25), i.e.

$$K = K_0 \chi \left[\frac{f_l^3}{(1-f_l)^2} \right] + K_0 (1-\chi) \left[\frac{f_l}{\sqrt{1-f_l}} \right], \tag{26}$$

where the first and second terms represent axial and cross-flow permeabilities, respectively. For example, $\chi = 0$ corresponds to a cross-flow and $\chi = 1$ represents an axial flow with the appropriate permeability factors employed in each limiting case.

In the previous studies, χ was computed in terms of the local temperature gradient. However, it is anticipated that an alternative entropy-based formulation provides important opportunities for applying previous

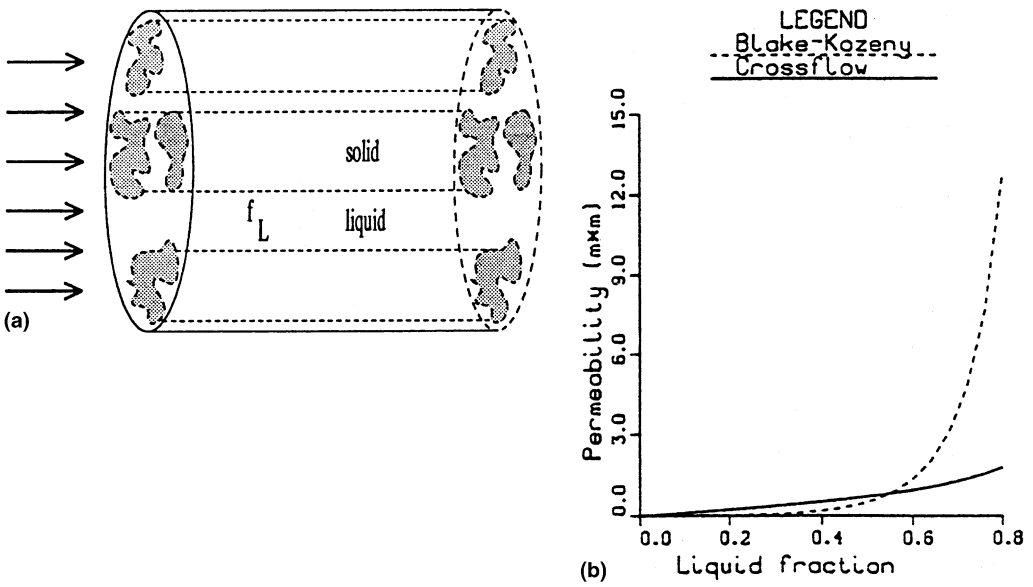

Fig. 3. (a) Permeability analogy for interdendritic axial conditions and (b) comparison between axial and cross-flow cases.

entropy advances (i.e. [14]) to the current interface tracking problem. The context of these advances involves applications to interfacial computations (i.e. momentum phase interaction terms). In particular, some possible opportunities include improved numerical stability, computational performance and other opportunities [19]. Since the direction of dendritic growth is related to the local thermal irreversibility, it is anticipated that entropy can be used to interpret axial and cross-flow contributions in the interdendritic permeability. As a result, we will consider a weighting between $\mathbf{v}$ relative to the dendritic growth direction based on thermal irreversibility and entropy.

In dendritic solidification, the primary dendrite arms grow in the direction of the local temperature gradient [21]. The gradient vector field gives the direction of steepest ascent (or descent for negative gradient vector). Since the primary dendrite arm growth is aligned with the local temperature gradient, then this growth occurs towards the steepest temperature slope. This direction corresponds to the maximum thermal irreversibility. This thermal irreversibility, $\dot{P}_{s,t}$, can be subdivided into x- and y-direction components, $\dot{P}_{s,tx}$ and $\dot{P}_{s,ty}$, respectively, in the following manner:

$$\dot{P}_{s,t} = \frac{k}{T^2}\left(\frac{\partial T}{\partial x}\right)^2 + \frac{k}{T^2}\left(\frac{\partial T}{\partial y}\right)^2 = \dot{P}_{s,tx} + \dot{P}_{s,ty}. \tag{27}$$

Although entropy production is a scalar, and not a vector field, we may define an equivalent entropy vector, $\hat{\mathbf{P}}_{s,t}$, consisting of the above components of entropy production in the x- and y-directions, given by $\dot{P}_{s,tx}\hat{\mathbf{i}}$ and $\dot{P}_{s,ty}\hat{\mathbf{j}}$ (note: unit vectors $\hat{\mathbf{i}}$, $\hat{\mathbf{j}}$), respectively. For example, a large component $\dot{P}_{s,tx}$ (in comparison to $\dot{P}_{s,ty}$) suggests that entropy production arises mainly from heat flow in the x-direction. Based on this concept, a flow alignment weighting factor is defined as follows:

$$\chi = \frac{\left|\mathbf{v}\sqrt{\hat{\mathbf{P}}_{s,t}}\right|}{|\mathbf{v}|\left|\sqrt{\hat{\mathbf{P}}_{s,t}}\right|}; \quad \sqrt{\hat{\mathbf{P}}_{s,t}} \equiv \sqrt{\dot{P}_{s,tx}}\hat{\mathbf{i}} + \sqrt{\dot{P}_{s,ty}}\hat{\mathbf{j}}, \tag{28}$$

where χ can be interpreted in terms of thermal irreversibility (or temperature gradient) relative to the direction of local interdendritic flow. The square root in Eq. (28) is adopted to maintain a more direct analogy between entropy production in Eq. (27) and temperature gradient (or heat flow).

In Fig. 3(b), a comparison involving the permeability variations for the axial (Blake–Kozeny) and cross-flow models with $K_0 = 1$ (sample reference case) is illustrated. At values of liquid fraction above approximately 0.5, it can be observed that the axial permeability exceeds the cross-flow value. In this case, the effective (overall) permeability in Eq. (26) is reduced by the weighting of the cross-flow component. As a result, a larger pressure difference associated with interdendritic flow may be realized in the current permeability model (in comparison to Blake–Kozeny model). It is anticipated that this additional cross-flow weighting can provide an important corrective mechanism in the computations.

The equivalent vector $\hat{\mathbf{P}}_{s,t}$ is similar to the heat flux vector, with two notable exceptions: (i) minus sign for Fourier heat flux; (ii) magnitude of $k|\nabla T^2|/T^2$, rather than $k|\nabla T|$. Otherwise, the physical interpretation of the permeability model remains that a higher cross-flow weighting is given when the interdendritic flow is normal to the direction of maximum thermal irreversibility (direction of dendritic growth). Conversely, the axial permeability is adopted when the velocity is aligned with the direction of the maximum thermal irreversibility. The anticipated benefit is that this entropy-based approach can provide improved accuracy for interface tracking during phase change processes.

3.3. Local reheating, recalescence and coarsening

During dendritic solidification, the released latent heat is transferred to the surrounding liquid–solid mixture, and if it exceeds the rate of external cooling, then a local temperature rise, or recalescence, may be observed. In addition with solute diffusion, this reheating may initiate melting of smaller dendrite arms at the expense of growing primary arms (i.e. dendritic coarsening). Coarsening during crystal formation and sedimentation in solidification processes may contribute to recalescence and latent heat release. In both cases, thermodynamic irreversibilities with entropy production arise during the heat transfer processes. Since reheating and coarsening may affect the final material properties, such as material strength, these processes are important concerns during solidification processing of many materials. It will be shown that entropy can serve as an effective variable in understanding these processes.

Consider a simplified heat balance for a crystal (or dendrite) during solidification. The transient temperature change arises from the net heat exchange with the surrounding solid–liquid mixture (described by overall heat transfer coefficient, h) and release of latent heat from the freezing crystal, i.e.

$$\rho\mathscr{V}c_p\frac{\partial T}{\partial t} = hA(T - T_f) - \rho\mathscr{V}\Delta e_f\frac{\partial f_l}{\partial t}, \tag{29}$$

where $\mathscr{V}$, A and T_f refer to a characteristic crystal (or dendrite) volume, corresponding surface area, and surrounding mixture temperature, respectively. Expanding the last derivative in Eq. (29) through the chain rule, we obtain

$$\frac{\partial T}{\partial t} = \frac{hA}{\rho\mathscr{V}c_p}\left[\frac{T - T_f}{1 + (\partial f_l/\partial T)\Delta e_f/c_p}\right]. \tag{30}$$

A characteristic length scale, L_c, may be represented by the ratio $\mathcal{V}/A$ (reciprocal appears in above equation).

We can write Eq. (30) in a dimensionless form by selecting appropriate reference scales for temperature and time (i.e. $t_{ref} = L_c^2/\alpha$). The dimensionless entropy, temperature and time, and Stefan number ($c_p\Delta T/\Delta e_f$) will be denoted by s^*, θ, t^* and Ste, respectively. Writing Eq. (30) in dimensionless form, we then obtain

$$\frac{\dot{\theta}}{\theta} = \frac{h' L_c}{k_l}\left(\frac{k_l}{k_s}\right) \equiv Nu\left(\frac{k_l}{k_s}\right), \tag{31}$$

where

$$h' = h\left[1 - \frac{1}{1 + Ste/(\partial f_l/\partial\theta)}\right] \tag{32}$$

refers to a modified heat transfer coefficient accounting for simultaneous external cooling and release of latent heat from the solidified crystal to the interdendritic fluid. Also, the dot notation in Eq. (31) represents differentiation with respect to time.

Upon comparing Eq. (31) with the rate of entropy change arising from the sensible heat portion of the Gibbs equation (i.e. Maxwell type relation where $c\,dT = T\,ds$), we have

$$\frac{\partial s^*}{\partial t^*} = \frac{\dot{\theta}}{\theta} = Nu\left(\frac{k_l}{k_s}\right). \tag{33}$$

The change of liquid fraction with temperature is calculated based on a suitable supplementary relation, such as an approximated linear variation of f_l with θ through the two-phase region. In a similar way as analogies between heat and momentum transport (i.e. Reynolds analogy), the above result indicates an analogy between heat and entropy. We will use this heat–entropy analogy for describing recalescence processes.

Also, the process of coarsening is closely related to recalescence during solid–liquid phase change. During coarsening, small or secondary dendrite arms (or crystals) shrink or melt at the expense of heat transferred from the large and growing main dendrites. The speed and mechanisms of coarsening are not well understood; the previous results suggest that entropy may serve as an effective variable in characterizing coarsening and recalescence. In the experimental studies, entropy is not measured directly, but rather indirectly through temperature measurements. Thus, the magnitude of recalescence will be observed by a measured temperature rise, and the corresponding dimensionless temperature gradient at the dendrite arm (characterized by Nusselt number) can be interpreted in terms of the local rate of entropy change. This entropy change (measured indirectly) incorporates heat flow from the interdendritic fluid, as well as latent heat released from the crystal or dendrite. Both mechanisms are important parts of understanding recalescence and coarsening during remelting of small, secondary dendrite arms.

We can obtain further information regarding effective heat transfer coefficient, h' (and Nu), by performing many phase change experiments involving different initial temperatures (leading to different Grashof numbers) and then seeking a suitable dimensionless correlation for Nusselt number, Nu, in terms of Grashof number, Gr, and other parameters. This is similar to the approach whereby single phase convection correlations are constructed for external or internal flows. For example, we can measure the initial and wall temperatures (with resulting Grashof number), and then find the entropy changes and other parameters during a specific phase change experiment. Then, the effective heat transfer coefficient can be estimated from Eq. (33). These experiments can then be repeated for other fluids/conditions and presented in a final correlated form.

In addition to the above heating modes during recalescence, the duration of recalescence may be estimated from a simplified one-dimensional heat and solute concentration analysis (see Appendix A). In particular, it may be shown that the recalescence duration, Δt, may be approximated in terms of interface position, $R(t)$, and partition ratio, k_p (i.e. C_s/C_l at interface), in the following manner:

$$\Delta t \approx \frac{D}{2(1-k_p)}\left[\left(\frac{\Delta e_f}{Qc_pR}\right)^2 - \left(\frac{1}{V_0}\right)^2\right] - \left[\frac{32D\pi\sigma^3}{6(1-k_p)k_B\Delta s^2 TV_0^2}\right]\Big/\Delta T^2 \equiv A - \frac{B}{\Delta T^2}, \tag{34}$$

where A and B are the "constants" indicated by the first and second set of square brackets, respectively. Also, k_B, Δs_f, σ and ΔT refer to Boltzmann's constant (1.38×10^{-23} J/K), entropy of fusion per unit volume, interface energy (J/m^2) and undercooling level (i.e. difference between chilled wall temperature and freezing temperature of liquid) prior to solidification.

The parameters Q and V_0 in Eq. (34) refer to approximate (uniform) cooling/heating rate and initial growth rate of crystal (or velocity corresponding to nucleation rate for crystal approximated as spherical particle), respectively. Although Q and V_0 vary throughout the mixture, the purpose of this analysis is merely an observation of general trends in Δt with respect to ΔT. In a similar way as empirical coefficients in other phase change correlations, such as empirical coefficients in the Rohsenow nucleate boiling correlation [22], the values V_0 and R (characteristic crystal size or dendrite dimension) can be correlated with various problem conditions.

In general, the result in Eq. (34) intersects the ΔT axis at $\Delta T_0 = \sqrt{B/A}$ and recalescence is not observed for $\Delta T \leqslant \Delta T_0$. Also, Eq. (34) indicates that the recalescence period increases with undercooling level, ΔT. It appears

that as ΔT increases, latent heat is released from the solidified material such that the duration of recalescence is extended. It is intended here that these types of trends, rather than detailed quantitative predictions, can be gained from the current recalescence analysis.

In this analysis, a uniform heating/cooling rate was assumed. Entropy can serve as an effective variable in the above formulation since this local heating/cooling rate can be related to the correlation involving heat transfer coefficient and entropy in Eq. (33). Thus, a heat–entropy analogy can provide an improved estimate of the relevant heating/cooling rate, based on the earlier result that the local Nusselt number is correlated with respect to the local rate of entropy change. In particular, the average heat transfer coefficient during this period can be estimated by integration over the range where a positive entropy derivative is observed in the data (i.e. conditions corresponding to recalescence and/or coarsening). In this way, the time period of recalescence can be expressed in terms of a heat–entropy analogy.

3.4. Numerical iterations

Although we have outlined the relevant entropy equations, the entropy values in a numerical formulation cannot be calculated until the phase distribution is known. Finding the phase in a finite control volume requires a solution of the energy equation, but this solution requires knowledge of the proper phase distribution. As a result, an iterative approach is required to find the proper phase distribution. An iterative procedure will now be described in conjunction with the Second Law. Unlike conventional procedures, such as Picard iteration, which may violate the Second Law by producing non-physical phase distributions (i.e. a solid region completely enclosed by liquid even though zero sources and sinks exist there in the pure material), the current procedure will be closely linked with the Second Law.

A primary difficulty with accurate predictions of solid–liquid phase change is interface tracking (i.e. predicting the location of the phase interface). The following rules will be used to estimate the tentative phases such that the solution of the energy equation can be obtained, and then repetitive iterations of these rules are performed until no further changes in spatial phase distribution occur at the current time step. It will be shown that these physically based iterations are closely linked with the general principle of non-decreasing entropy and the Second Law.

Rule 1. A control volume must pass through a melt region during phase transition between solid and liquid phases.

In order to prove this assertion, consider a situation where molecules align themselves on a crystal lattice from the liquid but no change of entropy occurs during the process. In other words, $\Delta s_{\mathrm{f}} = 0$ in Eq. (20) because the material passes from a liquid to solid phase without passing through the mushy (two-phase) region. However, under these circumstances, the right-hand side of Eq. (20) becomes negative and the Second Law is violated, thereby showing that the material must indeed pass through a two-phase region during phase transition. In reality, $\Delta s_{\mathrm{f}} > 0$ because we have more certainty regarding the whereabouts of a molecule in the solid phase as compared to the molecule's location in the liquid.

Rule 2. Phase transition in a control volume cannot occur without a phase transition to the same phase in an adjacent volume first.

In a similar manner, consider a proof by contradiction and assume instead that a solid region could form in isolation within the liquid even though no sources or sinks of energy exist within the domain. Also, we are considering phase transition in accordance with the phase equilibrium diagram such that solidification (or melting) occurs instantaneously at the equilibrium liquidus (or solidus) temperature. Under these assumptions, a solid volume could be established in between adjacent liquid volumes. Without considering concentration effects, this suggests that the temperature in the middle volume is lower than the surrounding liquid temperatures. However, in the case of conduction transport, energy flows down a temperature gradient and therefore Fourier's law is necessarily violated, because in this case, energy flows away from the middle volume (i.e. solidification occurs) yet it also travels up a temperature gradient. This situation cannot occur without additional effects such as energy sinks that would lead to this type of phenomenon. Alternatively, for the case of heat transfer alone, it can be shown from Eqs. (20) and (21) that a reverse direction of heat transfer (i.e. heat flux of $k\nabla T$ rather than $-k\nabla T$) leads to negative entropy production and a violation of the Second Law. The result is that the original assumption is invalid and a volume cannot change phase without a phase transition in adjacent volumes first.

Although the Second Law can be expressed in a variety of diverse qualitative ways, a quantitative measure is also an important aspect of the Second Law. In particular, the magnitude of entropy production characterizes the irreversible processes (i.e. viscous mixing, heat transfer) and diffusive (entropy-producing) or non-physical (entropy-destroying) parts of a numerical formulation. Thus, the following objective/rule is proposed in addition to the previous two rules.

Rule 3. (Objective) The tentative phase within a control volume must give a positive entropy production rate for the discrete time step.

This objective/rule provides a quantitative description of the Second Law whereas the previous two rules were viewed from a procedural perspective of the Second Law for phase change problems. Although the previous two rules alone do not ensure positive entropy production in the computations, it is anticipated that these rules provide effective guidelines for compliance with objective/rule 3 because the rules have been interpreted as discrete analogies of the Second Law.

Since the previous two rules are directly implemented in the specification of tentative phases prior to each computational iteration, then these Second Law analogies will not be violated. Thus, these two rules permit efficient phase-temperature iterations during phase change while effectively promoting compliance with the Second Law. It is anticipated that this approach could provide convergence acceleration as well as a unified and physically based understanding of discrete error analysis. Also, rather than ad hoc tolerances for solution convergence, these rules provide a basis from which rigorous analysis of non-linear stability for phase change problems can be obtained.

3.5. Non-linear stability

Although the previous heat–entropy analogies (involving momentum phase interactions, recalescence and phase rules) provide a physically based formulation, these analogies alone do not ensure stability of the numerical computations. However, compliance with the Second Law is closely related to non-linear stability since diverging (or oscillating) results, as well as negative entropy production, are non-physical processes. As a result, it is anticipated that the emphasis on entropy in this paper can foster developments leading to stable computations of heat transfer and fluid flow. In the following example, a specific case is presented to clearly identify a link between the Second Law and stable, converging numerical computations involving heat transfer.

3.5.1. Example. Liquids separated by adiabatic partition

In this example, two liquid mixtures are initially separated by a partition at the midpoint of a cavity (see Fig. 4(a)). The initial liquid temperature on the left-hand side exceeds the initial temperature on the right-hand side. Refer to Fig. 4(a) where the initial temperatures are T_1^0 and T_2^0, respectively, and the subscript and superscript refer to side and time step, respectively. Furthermore, we will assume that the mass and density of material are equal on both sides of the cavity.

Now the partition is removed and heat is transferred from the left to right side by conduction. The purpose of this example is to establish a relationship between the Second Law and computational stability by considering bounds on the solution norm. We will establish this objective without adopting specific numerical values in the example, and as a result, it is anticipated that the result can be generalized and extended to other problems, including problems with phase change.

Under these conditions, the final equilibrium temperature (after complete diffusion) is the arithmetic average of the two initial temperatures. As a result, we can calculate the entropy at the equilibrium state using the entropy equation of state. Recall that entropy, $S(\xi)$, can be written in terms of the vector of conserved variables, ξ (i.e. energy, or temperature, in this example), through the Gibbs equation. Also, from the downward concavity property of the entropy function, the derivative $S'(\xi)$ is decreasing as it approaches the equilibrium state, $\overline{\xi}$. Expressing this decrease in mathematical terms, we obtain

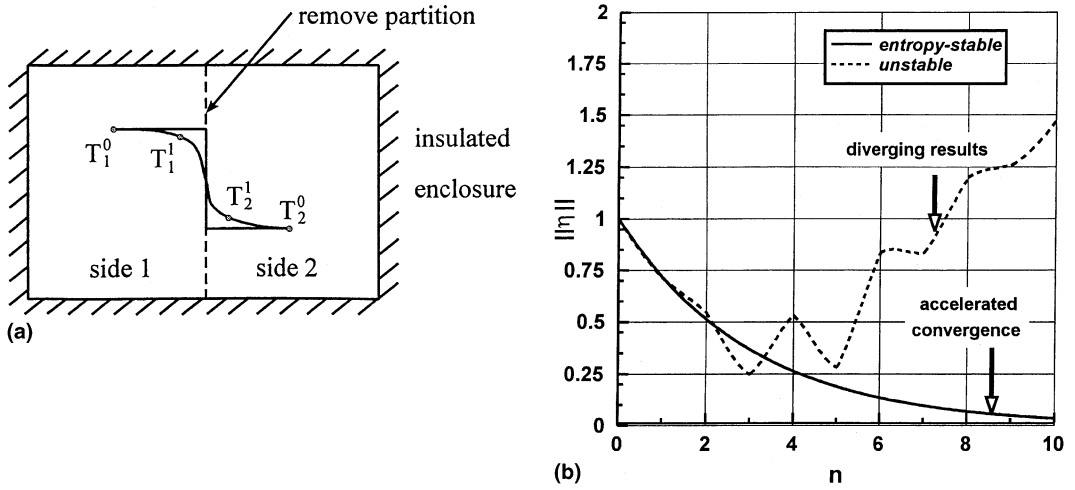

Fig. 4. Example (a) schematic and (b) convergence characteristics.

$$S(\overline{\xi}) - S(\xi_i) - S'(\overline{\xi})(\overline{\xi} - \xi_i) \geqslant 0, \tag{35}$$

where the equality holds at the equilibrium state, $\xi = \overline{\xi}$, and the subscript i refers to node i in a spatial discretization of the problem domain.

A measure of the thermodynamic state of the entire system relative to the reference condition at $\overline{\xi}$ is obtained by averaging Eq. (35) over the spatial domain. At time step n, we obtain

$$\begin{aligned}\langle \Delta S \rangle^n &= \langle S(\overline{\xi}) - S(\xi_i) - S'(\overline{\xi})(\overline{\xi} - \xi_i) \rangle \\ &= S(\overline{\xi}) - \langle S(\xi^n) \rangle \geqslant 0,\end{aligned} \tag{36}$$

where the averaging operator, $\langle \xi \rangle$, is the average value of ξ (spatially averaged across entire domain). Also, the latter averaged term in Eq. (35) vanished since it was averaged to zero.

Based on the Second Law for the insulated enclosure, we find that the total entropy increases, and as a result, the entropy difference (relative to highest entropy at final equilibrium state) decreases with time. For example, after a single time step,

$$\langle \Delta S \rangle^0 \geqslant \langle \Delta S \rangle^1 \geqslant 0. \tag{37}$$

The above entropy differences can be computed from the entropy equation of state. In this example, a piecewise logarithmic equation of state based on the Gibbs equation [19] is adopted.

After substituting the specific form of the equation of state into Eq. (37), taking exponents of all resulting logarithmic terms, and rearranging, we obtain

$$|\overline{T} - T_1^1| + |\overline{T} - T_2^1| \leqslant |\overline{T} - T_1^0| + |\overline{T} - T_2^0|, \tag{38}$$

where the absolute values can be interpreted in a geometric way. The temperature differences relative to the equilibrium temperature, $\overline{T}$, can be interpreted as norms or "distances" from the equilibrium state. In particular, let us define $\|\eta\|_1$ as the L_1 norm of a scalar η, such as ΔT, where

$$\|\eta\|_1 \equiv \left(\frac{1}{N} \sum_{i=1}^{N} |\overline{T} - T_i| \right), \tag{39}$$

and N refers to the total number of control volumes (i.e. $N = 2$ may be adopted in our example for two sides of the enclosure).

If we now extend and generalize the result in Eq. (38) by taking T_1^1 and T_2^1 as the initial conditions (rather than T_1^0 and T_2^0) prior to the second time step, and similarly with the third time step, and so on, we obtain

$$\|\eta^n\|_1 \leqslant \|\eta^{n-1}\|_1 \leqslant \cdots \leqslant \|\eta^0\|_1. \tag{40}$$

This result suggests numerical stability with reference to the L_1 norm. Although this result was based on the downward concavity property of the entropy function in Eq. (35), it can be readily shown that the same result would be achieved through a direct application of the Second Law to both sides of the enclosure. As a result, it can be observed that compliance with the Second Law (or the equivalent principal of non-decreasing entropy in this example) ensures that the L_1 norm of the scalar remains bounded. In other words, an entropy-based approach has ensured numerical stability since the temperature difference (with respect to equilibrium temperature) is decreasing in a monotonic fashion.

The following expressions give two examples of functions related to Eq. (40): (i) an entropy-stable function (subscript es) satisfying the inequalities in Eq. (40); (ii) an unstable function (subscript us) exhibiting non-bounded (oscillatory) solution norms not obeying Eq. (40), i.e.

$$\eta_{\text{es}} = \exp\left(-\frac{n}{3} \right), \tag{41}$$

$$\eta_{\text{us}} = \exp\left(-\frac{n}{3} \right) \left| 1 + 0.004 n^4 \cos(n\pi) \right|. \tag{42}$$

These examples are illustrated in Fig. 4(b), where the solid and dashed lines represent the entropy-stable and unstable results, respectively. In the entropy-stable case, the solution norm is bounded by its initial value and it decreases in a monotonic fashion. This trend is a desirable characteristic of a numerical scheme since it provides a stable convergence in the computations. On the other hand, the unstable (oscillatory) result, η_{us}, illustrated by the dashed line in Fig. 4(b), does not obey the bounded condition in Eq. (40). As a result, the solution norm initially decreases but oscillations appear shortly thereafter and unstable computations appear in the results. Thus, a scheme which satisfies the inequality in the Second Law is more desirable since it provides stable computations.

Similar results involving gas dynamics have been reported by Camberos [23]. The main goal of this example is that we have established a relationship between the Second Law and solution stability. Although this example has not implemented phase change, it is given here to demonstrate some connections between entropy and stable temperature computations. Also, heat–entropy analogies have been adopted in the phase change models, but the overall formulation has not ensured compliance with the Second Law since negative entropy production may arise from discretization errors, etc. in the computations. However, it is anticipated that the entropy-based focus in various components of the model provide a solid basis from which this objective (compliance with Second Law) can be achieved.

4. Conclusions

Analogies between heat and entropy transport have been presented for problems involving solid–liquid

phase change. The interfacial entropy constraint gives the rate of entropy production at the moving interface due to viscous dissipation and heat and mass transfer. It is shown that the thermal irreversibility can be used in a permeability weighting factor in the two-phase zone for evaluation of phase interactions in the momentum equations. Also, recalescence and coarsening processes were examined in view of a heat–entropy analogy involving the rate of entropy change and local reheating due to the release of latent heat from a solidified crystal (or dendrite arm). Heat–entropy analogies were also presented for effective numerical computations of phase change heat transfer. In summary, it is anticipated that entropy can serve as an effective variable in describing and understanding various interfacial processes during solid–liquid phase change.

Acknowledgements

The work in this paper was supported, in part, by a research grant from the Natural Sciences and Engineering Research Council of Canada to the author.

Appendix A. Duration of recalescence

For a control volume moving at a velocity $V(t)$ with the phase interface in a one-dimensional, semi-infinite domain, we have the following approximated set of governing equations and interfacial constraints:

$$\frac{\partial C}{\partial t} = D\frac{\partial^2 C}{\partial x^2}, \tag{A.1}$$

$$\rho c_p \frac{\partial T}{\partial t} = k\frac{\partial^2 T}{\partial x^2} - \rho \Delta e_f \frac{\partial f_l}{\partial t}, \tag{A.2}$$

subject to

$$C_l(0) = C_0, \quad T(0) = T_0; \tag{A.3}$$

$$-D\frac{\partial C}{\partial x}\bigg|_R = C_l(1-k_p)V, \quad C_l|_\infty = C_0; \tag{A.4}$$

$$-k\frac{\partial T}{\partial x}\bigg|_l + k\frac{\partial T}{\partial x}\bigg|_s = \rho V \Delta e_f, \quad T|_\infty = T_0; \tag{A.5}$$

where $R(t)$ is the interface position and the subscript ∞ refers to a location sufficiently far from the moving phase interface where the bulk liquid concentration, C_0, and temperature, T_0, are observed.

Integrating Eq. (A.1) from $x = R \to \infty$,

$$\frac{\partial}{\partial t}\int_R^\infty C_l(x,t)\,dx = C_l(1-k_p)V(t). \tag{A.6}$$

An exponential concentration profile is assumed in the liquid region ahead of the interface [24], i.e.

$$C_l = \frac{C_0}{k_p}\exp\left[-V(t)\left(\frac{x-R}{D}\right)\right]. \tag{A.7}$$

Combining Eqs. (A.6) and (A.7), we obtain the following first-order differential equation for $V(t)$:

$$\frac{dV}{dt} + \left(\frac{1-k_p}{D}\right)V^3 = 0. \tag{A.8}$$

Solving Eq. (A.8) subject to $V(0) = V_i$, we obtain

$$V(t) = V_i\sqrt{\frac{1}{1+\kappa t}}; \quad \kappa = \frac{2(1-k_p)}{D}V_i^2. \tag{A.9}$$

As the solution approaches a steady state ($t \to \infty$), conduction into the interface balances the latent heat release from the interface and the interface becomes stationary, i.e. $V(t) \to 0$ in Eq. (A.9).

The rate of temperature change with time is negative during cooling, but it may become zero and positive during recalescence if the rate of release of latent heat exceeds the rate of cooling. In the case of a uniform heating/cooling rate, Q, the onset and completion of recalescence can be estimated from Eqs. (A.2) and (A.9) at a zero rate of temperature change, i.e.

$$\frac{\partial T}{\partial t} \approx -Q + \frac{\Delta e_f}{c_p}\left[\frac{V_i}{R}\sqrt{\frac{1}{1+\kappa t}}\right] = 0. \tag{A.10}$$

As a result, the following duration of recalescence is obtained,

$$\Delta t = \frac{D}{2(1-k_p)}\left[\left(\frac{\Delta e_f}{Qc_pR}\right)^2 - \left(\frac{1}{V_i}\right)^2\right]. \tag{A.11}$$

Under the assumption that the initial crystal growth rate, V_i, varies in an exponential manner [25] as a function of the interface Gibbs energy, ΔG, we have

$$V_i = V_0\exp\left(-\frac{\Delta G}{k_B T}\right), \tag{A.12}$$

where $k_B = 1.38 \times 10^{-23}$ J/K is the Boltzmann constant and ΔG represents the energy required to maintain crystal bonds in the lattice structure from melting back to the liquid. The Gibbs energy may be written in terms of the interface energy, σ (J/m^2), and the entropy of fusion per unit volume, Δs_f (J/m^3 K), in the following manner:

$$\Delta G \approx \frac{16\pi}{3}\frac{\sigma^3}{\Delta s_f^2 \Delta T^2}, \tag{A.13}$$

where ΔT is the undercooling level prior to the onset of solidification.Substituting Eqs. (A.12) and (A.13) into Eq. (A.11),

$$\Delta t \approx \frac{D}{2(1-k_p)}\left[\left(\frac{\Delta e_f}{Qc_pR}\right)^2 - \left(\frac{1}{V_0}\right)^2\right] - \left[\frac{D}{2(1-k_p)}\frac{32\pi\sigma^3}{3k_B\Delta s^2 TV_0^2}\right]\Big/\Delta T^2 \equiv A - \frac{B}{\Delta T^2}. \quad (A.14)$$

This result is adopted as the approximate duration of recalescence (Section 3.3).

References

[1] M. Salcudean, R.I.L. Guthrie, A three dimensional representation of fluid flow induced in ladles or holding vessels by the action of liquid metal jets, Metall. Trans. B 10b (1979) 423–428.

[2] E. Pardo, D.C. Weckman, A fixed grid finite element technique for modelling phase change in steady state conduction – advection problems, Int. J. Numer. Meth. Eng. 29 (1990) 969–984.

[3] W.D. Bennon, F.P. Incropera, Numerical analysis of binary solid–liquid phase change using a continuum model, Numer. Heat Transfer 13 (1988) 277–296.

[4] G.F. Naterer, G.E. Schneider, PHASES model of binary constituent solid–liquid phase transition – Part 1. Numerical method, Numer. Heat Transfer B 28 (2) (1995) 111–126.

[5] G.F. Naterer, G.E. Schneider, PHASES model of binary constituent solid–liquid phase transition – Part 2. Applications, Numer. Heat Transfer B 28 (2) (1995) 127–137.

[6] S.C. Flood, P.A. Davidson, Natural convection in aluminum direct chill cast ingot, Mater. Sci. Technol. 10 (1994) 741–751.

[7] M.A. Rady, V.V. Satyamurty, A.K. Mohanty, Thermosolutal convection and macrosegregation during solidification of hypereutectic and hypoeutectic binary alloys in statically cast trapezoidal ingots, Metall. Mater. Trans. B 28B (1997) 943–952.

[8] A.L. Maples, D.R. Poirier, Convection in the two-phase zone of solidifying alloys, Metall. Trans. 15B (1984) 163–172.

[9] G.F. Naterer, Simultaneous pressure–velocity coupling in the two-phase zone for solidification shrinkage in an open cavity, Modelling and Simulation in Mater. Sci. Eng. 5 (6) (1997) 595–613.

[10] M. Salcudean, Z. Abdullah, On the numerical modelling of heat transfer during solidification processes, Int. J. Numer. Meth. Eng. 25 (1988) 445–473.

[11] A. Bejan, Entropy Generation Minimization: The Method of Thermodynamic Optimization of Finite-time Systems and Finite-time Processes, CRC Press, Boca Raton, 1996 (Chapter 8).

[12] C. Charach, I.L. Rubinstein, On entropy generation in phase-change heat conduction, J. Appl. Phys. 66 (9) (1989) 4053–4061.

[13] P.D. Lax, Shock waves and entropy, Contributions to Non-linear Functional Analysis, Academic Press, New York, 1971, pp. 603–634.

[14] G.F. Naterer, Constructing an entropy-stable upwind scheme for compressible fluid flow computations, AIAA J. 37 (3) (1999) 303–312.

[15] G.F. Naterer, G.E. Schneider, Use of the second law for artificial dissipation in compressible flow discrete analysis, AIAA J. Thermophys. Heat Transfer 8 (3) (1994) 500–506.

[16] W.J. Minkowycz, E.M. Sparrow, G.E. Schneider, R.H. Pletcher, Handbook of Numerical Heat Transfer, Wiley, 1988 (Chapter 8).

[17] G.E. Schneider, M.J. Raw, An implicit solution procedure for finite difference modelling of the Stefan problem, AIAA J. 22 (1984) 1685–1690.

[18] G.F. Naterer, Numerical and experimental techniques for binary solid–liquid phase transition, Ph.D. Thesis, Department of Mechanical Engineering, University of Waterloo, Canada, 1995 (Chapter 4).

[19] G.F. Naterer, Predictive entropy based correction of phase change computations with fluid flow – Part 1: second law formulation, Numer. Heat Transfer B 37 (4) (2000) 393–414.

[20] R. Bird, W. Stewart, E. Lightfoot, Transport Phenomena, Wiley, New York, 1960.

[21] M.C. Flemings, Solidification Processing, McGraw-Hill, New York, 1974 (Chapter 5).

[22] F.P. Incropera, D.P. DeWitt, Fundamentals of Heat and Mass Transfer, fourth ed., Wiley, New York, 1996 (Chapter 10).

[23] J.A. Camberos, A probabilistic approach to the computational simulation of gas dynamic processes, Ph.D. Dissertation, Stanford University, 1995.

[24] C. Charach, Y. Keizman, Mass balance integral solution for planar solidification of diluted binary alloys with solute trapping effects, Computational Modelling of Free and Moving Boundary Problems vol. 3, Computational Mechanics Publications, 1995, pp. 157–164.

[25] W. Kurz, D.J. Fisher, Fundamentals of Solidification, Trans. Tech Publications, Switzerland, 1989 (Chapter 2).